Int. J. Electrochem. Sci., 9 **(2014)** 2631 - 2648

International Journal of ELECTROCHEMICAL SCIENCE
www.electrochemsci.org

Case study: Corrosion Behavior of Constructive Alloys in Linear Alpha Olefin Environment

Mohammed A. Amin[1,2,], Q. Mohsen[1], Nasser Y. Mostafa[1,3], Nader El-Bagoury[1,4], Abdullah Al-Refaie[5], Avtandil K. Bairamov[6], Saad Al-Maaesab[6], Esteban Morales Murillo[6], Saad Ayed Al-Qahtani[7]*

[1]Materials and Corrosion Lab, Chemistry Department, Faculty of Science, Taif University, 888 Hawiya, Saudi Arabia
[2] Chemistry Department, Faculty of Science, Ain Shams University, P.O. Box 11566, Abbassia, Cairo, Egypt.
[3] Chemistry Department, Faculty of Science, Suez Canal University, Ismailia, Egypt
[4] Casting Technology Lab., Manufacturing Technology Dept., Central Metallurgical Research and Development Institute, CMRDI, P. O. Box 87 Helwan, Cairo, Egypt.
[5]Corporate Research and Innovation Center (CRI), Saudi Basic Industries Corporation (SABIC), P.O. Box 4545-4700, Thuwal 23955-6900, Saudi Arabia
[6] Materials and Corrosion Section, SABIC Technology Center, P.O. Box #11669, Jubail Industrial City 31961, Saudi Arabia
[7]LAO Operation Department, Jubail United Petrochemical Company, P.O. Box: 10085, Jubail Industrial City 31961, Saudi Arabia
[*]E-mail: maaismail@yahoo.com
CC: nanotechnology2000@yahoo.com

Received: 3 October 2013 / *Accepted:* 10 January 2014 / *Published:* 2 March 2014

During initial days of α-SABLIN (LAO's) commercial plant operation, general corrosion was observed in the downstream separation columns. This was due to traces of catalyst not being completely neutralized thus forming acidic medium (mainly hydrochloric), resulting in the corrosion of the columns. In this respect the high temperature corrosion behavior of three important steel materials, namely carbon steel (CSA516) and ferritic (SS410) and austenitic (SS304L) stainless steels was studied by mass loss method at the process conditions and environment of the α-SABLIN (LAO's) commercial plant. Measurements were conducted at 270 ^{o}C and 29 bar as a function of immersion time (up to 30 days). Such measurements are complemented with X-ray diffraction (XRD), optical microscope (OM) and scanning electron microscopy (SEM). The obtained findings revealed that the three tested steel samples corrode in the environment of the α -SABLIN (LAO's) commercial plant. The corrosion rate varies depending on the steel chemical composition, with SS304L being the most corrosion-resistant among the tested samples.

Keywords: High temperature corrosion, Carbon steel, Stainless steel, α -SABLIN, Linear Alpha Olefins, (LAO).

1. INTRODUCTION

Linear alpha olefins are a range of industrially important alpha-olefins, including 1-butene, 1-hexene, 1-octene, 1-decene, 1-dodecene, 1-tetradecene, 1-hexadecene, 1-octadecene and higher blends of C_{20}-C_{24}, C_{24}-C_{30}, and C_{20}-C_{30} ranges. Industrially, linear alpha olefins are commonly manufactured by two main routes: oligomerization of ethylene and by Fischer-Tropsch synthesis followed by purification. Another route to linear alpha olefins which has been used commercially on small scale is dehydration of alcohols. Prior to about the 1970s, linear alpha olefins were also manufactured by thermal cracking of waxes, whereas linear internal olefins were also manufactured by chlorination/dehydrochlorination of linear paraffins [1].

HCl formation during α-SABLIN (LAO's) commercial plant operation can be considered as the main reason for the production of organic chloride as well as of alkylated toluene by Friedel-Crafts-alkylation reaction. The HCl and organic chloride formation affect the LAO product quality and generates major corrosion problems (Fig. 1) at the separation section downstream. Consequently, the LAO plant is subjected to many inspection shutdowns. This in turn affects the sustainability of the plant operation.

Figure 1. Photographs show the corrosion damages on different plant locations.

The objective here is to study the high temperature corrosion behavior of three important steel materials namely carbon steel (CSA516), ferritic (SS410) and austenitic (SS304L) stainless steels in α-SABLIN (LAO's) solution based on a mass loss method. Measurements were conducted as a function of immersion time using an Autoclave at 270 ^{o}C and 29 bar. These are complemented with substrate analysis using OM and SEM. X-ray Diffraction (XRD) studies were used to analyze the corrosion products.

The importance of such study is rendered necessary by the wide use of these steel alloys in different types of constructions and industries. In addition, these steels are currently used in the construction of the α -SABLIN (LAO's) commercial plant. Therefore, the purpose of this work is to compare the high temperature corrosion behavior of three tested alloys in order to select the proper alloy, based on the obtained corrosion data, to be used as a constructional material for the most vital and important parts (those subjected to severe corrosion) of the α -SABLIN (LAO's) commercial plant.

The high corrosion resistance of the selected alloy is expected to overcome the drawback of side reactions and HCl formation during catalyst deactivation. This shall assure no corrosion, as illustrated in Fig. 1, which was caused by the degradation of formed organic chloride and HCl reforming under elevated temperature at the bottom of separation section.

2. EXPERIMENTAL

The tested samples employed in this work are circular coupons of carbon steel (A516-70) and stainless steels (410 SS and 304L), as shown in Fig. 2.

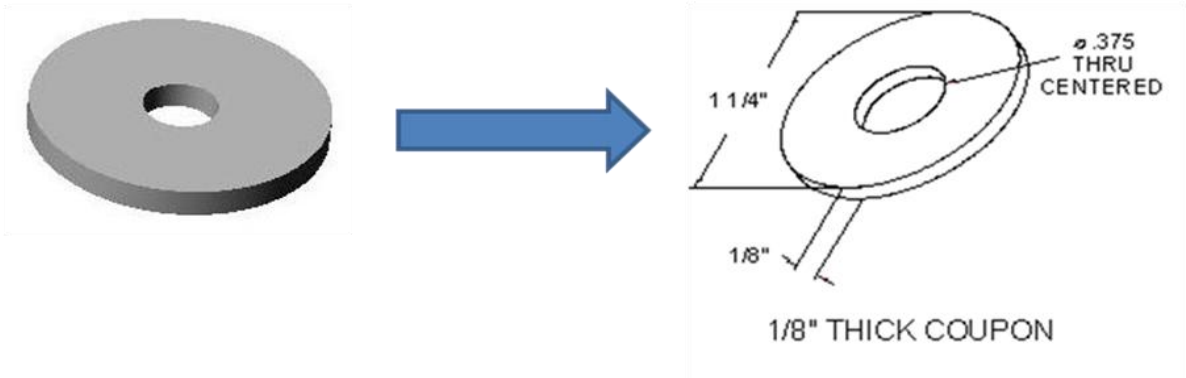

Figure 2. The circular coupon used in corrosion testing

The chemical composition of the three tested samples is presented in Table 1. The test solution is provided by plant, and used as received.

Table 1 – Chemical composition of the three tested steel samples.

Alloy	Alloying elements (%)					
	C	**Si**	**Mn**	**Cr**	**Ni**	**Fe**
CSA516-70	0.18	0.13	0.18	0.00	0.00	bal.
SS410	0.15	0.48	0.35	12.59	0.50	bal.
SS304L	0.03	0.46	0.73	18.43	7.91	bal.

The high temperature corrosion behavior experiments of the three tested samples were performed in a Teflon-lined steel Autoclave of 400 cm^3 capacity (closed environment in which the corrosive medium does not re-circulate) equipped with magnetic stirrer and heat controller, as shown in Figs. 3-5.

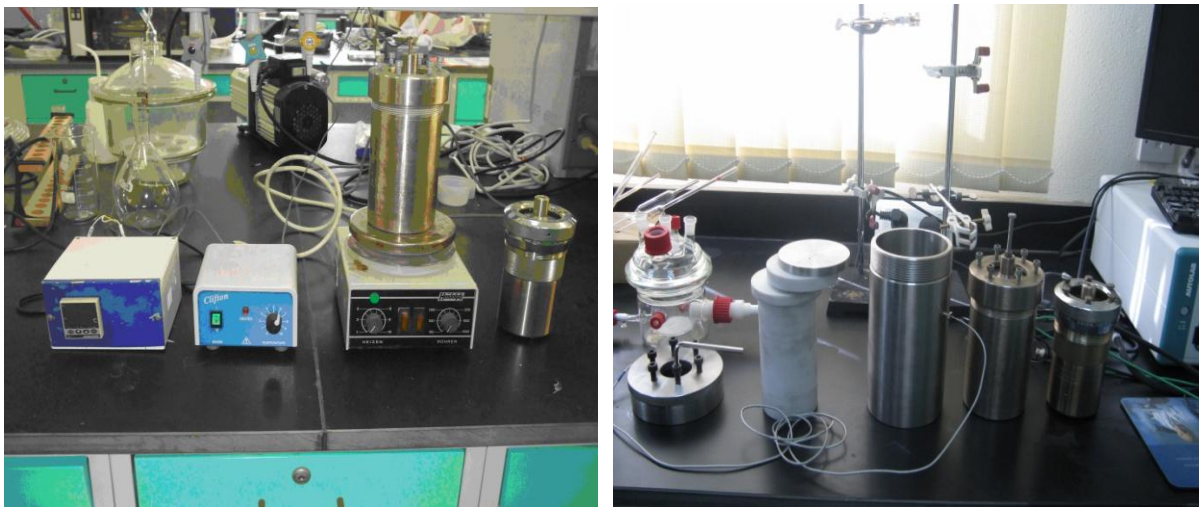

Figure 3. In-house built autoclave with heat controller and magnetic stirrer.

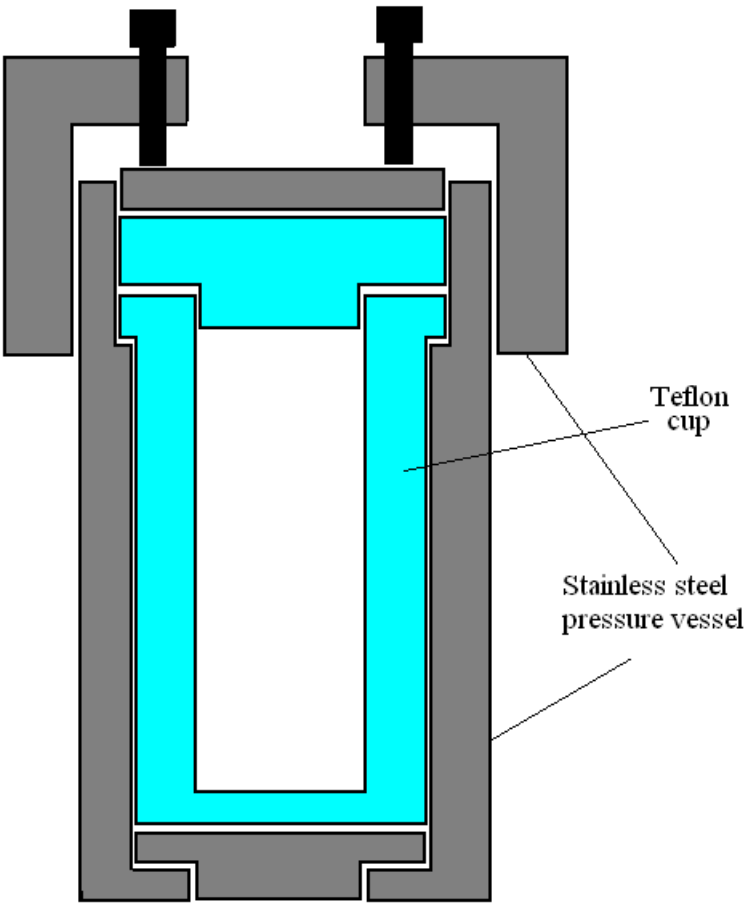

Figure 4. The autoclave cell.

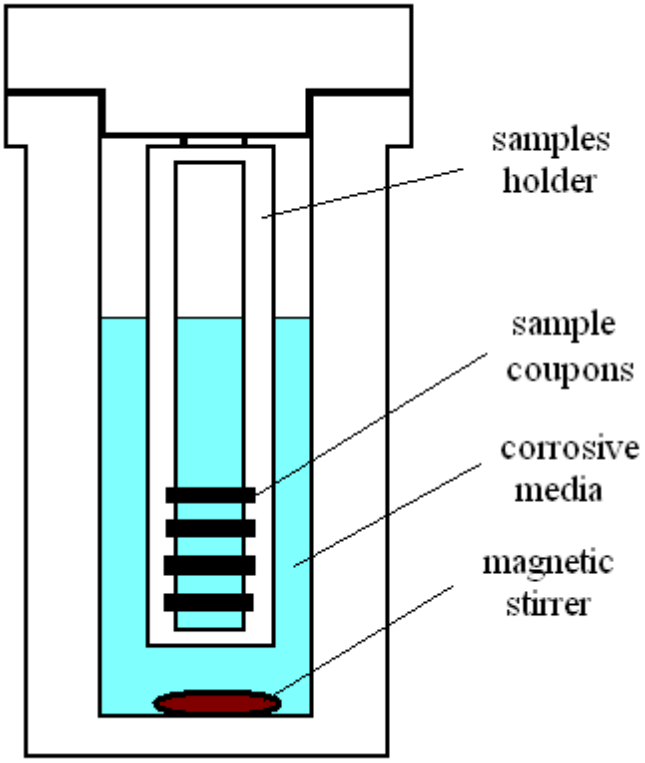

Figure 5. The inside Teflon cup with Teflon coupons holder.

The high temperature tests were carried out at 270°C and 29 bar to simulate the conditions of the LAO reactor.

Prior to each experiment, the tested samples were first grounded using 1200# grit SiC paper and then ultrasonically cleaned in ethanol. Two samples were used in each test for data repeatability. After filling the autoclave with the test solution, the coupons were immersed and fixed in a Teflon holder, Fig. 5. The autoclave was heated by three heater bands, which brought the temperature up to 270^{o}C.

Corrosion rates were calculated based on the mass changes of the samples. The mass change measurements were conducted by an analytical electron balance (0.0001 g in accuracy). Mass loss measurements were performed in a manner consistent with the ASTM G1 [2]. The corrosion behavior of coupon specimens was evaluated by measuring the mass loss as a function of the immersion time (3, 7, 14 and 30 days).

After the high temperature corrosion test has been completed at any given immersion time, corrosion products were removed adopting a cleaning procedure based on ASTM G1 [2].

The cleaning procedure was repeated on samples several times to reach steady state. The cleaning procedure was repeated here at least 7-10 times, and the mass loss was determined after each cleaning by weighing the samples. Finally, the mass loss was graphed as a function of the number of cleaning cycles to get the mass of the corrosion products, see later. The composition of the bath used in the cleaning procedure is: 0.5 L HCl (sp gr 1.19) + 3.5 g hexamethylene tetramine + 1L H_2O [2].

The morphologies of the corroded surfaces of the three tested samples were examined by an optical microscope (Metallurgical Microscope MX 7520, Camera Infinity 1, MEIJI TECHNO CO.

LTD, JAPAN) and an Scanning Electron Microscope (SEM; Analytical Scanning Electron Microscope JEOL JSM 6390 LA) after 30 days of immersion in the LAO test solution at 270 ^{o}C and 29 bar.

XRD studies (using a Cu target; the scan speed was 2.0^{o}/min and the 2θ angle ranged from 4^{o} to 90^{o}) were carried out for the corrosion products of the three tested alloys after 30 days of immersion to identify the chemical constituents of the accumulated corrosion products.

3. RESULTS AND DISCUSSION

3.1. Effect of cleaning cycles on mass loss of the corrosion products

Mass loss (Δm) coupon method is used to enable the corrosion rate measurements to be done without disturbing the plant operation. Moreover, this technique allows visual examination, physical measurements and the chemical analysis of the corrosion products.

In mass loss experiments, to avoid the accumulation of corrosion products, the preferred minum ratio of test solution to test specmin surface area is 15 mL/cm^2 [3]. Indeed, corrosion products could significantly affect the kinetics of mass loss, which is a measure for the uniform corrosion rate. During mass loss measurements against time, the absence of corrosion products (particularly if they are readily soluble) would yield Δm *vs.* time linear plots [4-8], and in other cases give straight lines pass through the origin, fitting the rate law for zero order reaction (i.e., uniform type of corrosion and constant corrosion rate over time) [9-23]:

$$\Delta m \text{ (or uniform corrosion rate)} = k\,t \qquad (1)$$

where k is the zero order rate constant, which is a measure for the uniform corrosion rate, and t refers to the immersion time.

For instance, Abiola and Otaigbe [10] studied the effects of *Phyllanthus amarus* extract on corrosion and kinetics of corrosion of Al in 2 M NaOH solutions using weight loss measurements. Authors in [10] reported that a zero-order kinetics relationship with respect to Al was obtained with and without the extract from the kinetics treatment of the weight loss data.

M. Abdallah and his coworkers [13-15] also obtained, during their corrosion and corrosion control studies of aluminium in hydrochloric acid solutions using some organic inhibitors, weight loss *vs.* time plots with typical straight lines passing through the origin (zero-order kinetics). Our research group [18-23] and others [9,16,17] came to the same findings and obtained weight loss (or uniform corrosion rate) *vs.* time plots with zero-order kinetics.

On the other hand the presence, or even incomplete removal, of corrosion products causes WL *vs.* time plots deviate from linearity; well documented in the literature; see for example *Refs.* [24-32].

In the present work, the ratio of the LAO test solution to the tested specimen surface area is about 60 mL/cm^2. However, after immersion in the test solution, the tested specimens, particularly alloy CSA516, showed adherent corrosion products built on their surfaces. The degree of scaling from one specimen to other differs, as will be seen and fully discussed in section 4.3, depending upon immersion time and composition of the tested sample.

Corrosion product removal procedures can be divided into three general categories: (i) mechanical, (ii) chemical and (iii) electrolytic. Following literature [2], an ideal procedure should remove only corrosion products and not result in removal of any base metal; see more details in the experimental section.

Figures 6a-6c are representative examples for the mass loss of the corrosion products as a function of the number of the cleaning cycles.

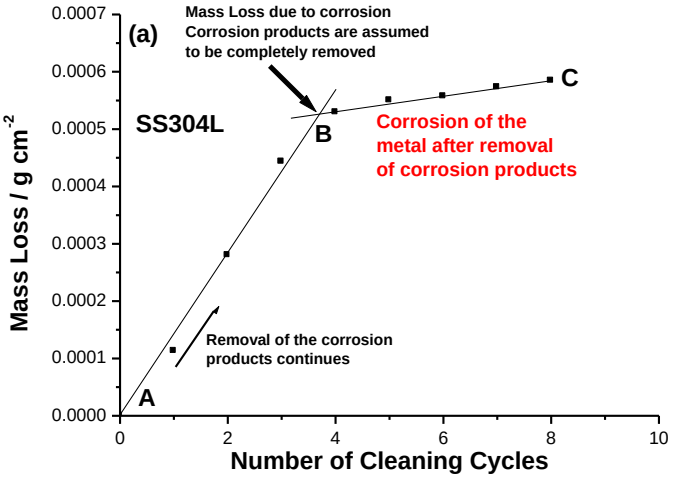

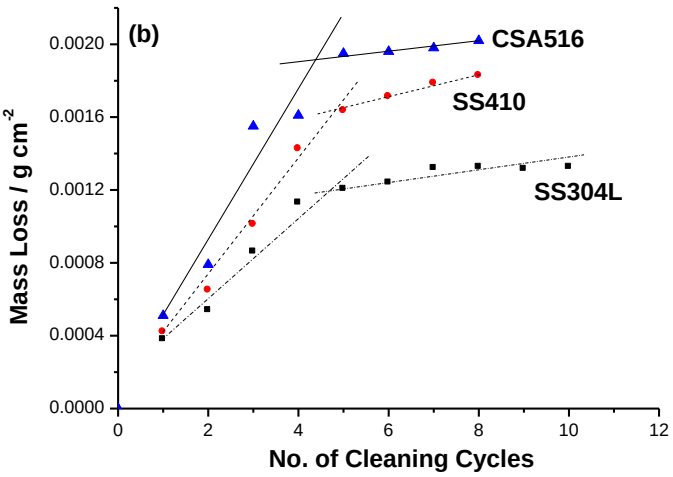

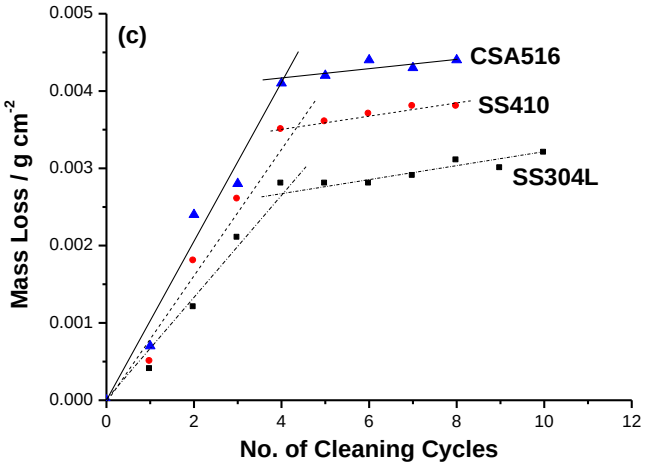

Figure 6. Mass loss *vs.* number of cleaning cycles recorded for the tested samples in the LAO's commercial plant test solution at 270 ^{o}C and 29 bar, as a function of the immersion time. (a) SS304L after immersion for 3 days in the test solution (b) the three tested samples after immersion for 14 days in the test solution (c) the three tested samples after immersion for 30 days in the test solution

It follows from Figs. 6a-6c that two straight line portions, namely AB and BC with different slopes were obtained. The slope of the portion BC is much smaller than that of the portion AB. The profile of such figures reveals the formation of a surface film due to corrosion (corrosion products) on the corroded surfaces [2].

Removal of the corrosion products starts from point A and continues up to point B (the point of intersection of the two straight portions), where corrosion products are assumed to be completely removed. Therefore, the portion following AB, namely BC represents corrosion of the bare alloy surface after removal of corrosion products. Thus, the mass loss at point B is due to the corrosion products, and can be taken as a correction factor (designated here as m_{cf}) for mass loss measurements, based on Eq. (2):

$$\text{Actual mass loss } (\Delta m) = m_{initial} - (m_{final} + m_{cf}) \quad (2)$$

Where $m_{initial}$ is the initial mass (mass of the sample before the corrosion test), m_{final} is the final mass (mass of the sample after the corrosion test; the sample is simply dried, but not chemically treated for the corrosion products, i.e., no cleaning process), and m_{cf} (our target) is the mass of the corrosion products.

The mass loss data were used to calculate the average corrosion rates, in mpy (Mils per year), for the three tested samples in the LAO test solution at 270 ^{o}C and 29 bar using Eq. 3 [2].

$$\text{Corrosion Rate (mpy)} = (K \times \Delta m)/(A \times T \times D) \quad (3)$$

where K is a corrosion constant [2], Δm is the mass loss in grams, D is the metal density in g cm^{-3}, A is the area of sample in cm^{2}, and T is the time of exposure of the metal sample in hours

The obtained corrosion rates are depicted in Fig. 7 for the three tested samples as a function of the immersion time.

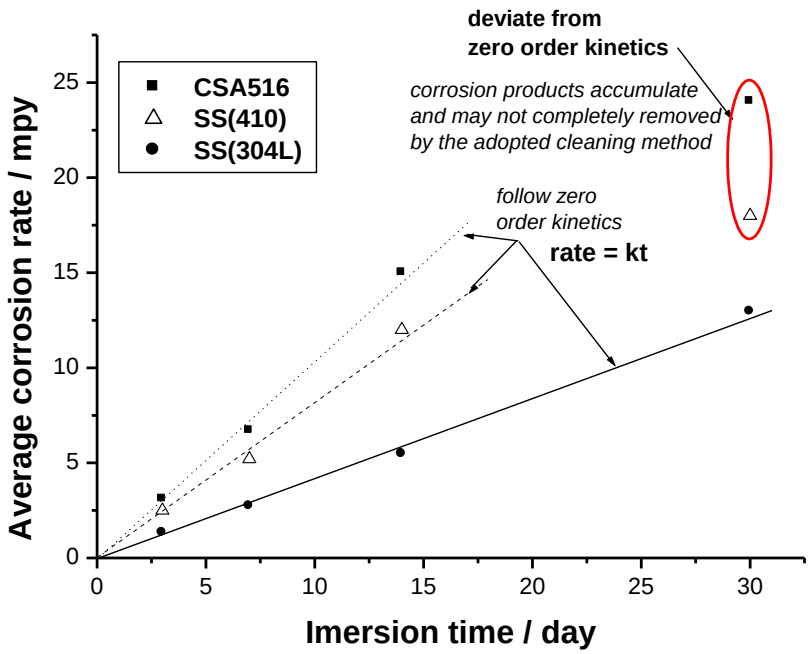

Figure 7. Average corrosion rates *vs.* immersion time of the three tested samples in the LAO's commercial plant test solution at 270 ^{o}C and 29 bar.

It follows that, at any given immersion time, the corrosion rate of the three tested samples decreases following the order: CSA516 > SS410 > SS304L.

Further inspection of Fig. 7 reveals that the average corrosion rates of CSA516 and SS410 follow the kinetics of zero order reaction, Eq. 1, up to 14 days of immersion. Deviation from zero order kinetics is quite clear at longer immersion (30 days of immersion), where corrosion products accumulate and may not completely removed by the adopted cleaning method [2].

On the other hand, the average corrosion rates recorded for SS304L fit well the kinetics of zero order reaction over the entire immersion time (i.e., up to 30 days of immersion). This is expected as the surface of SS304L is almost free from corrosion products, even after 30 days of immersion in the corrosion test solution.

4.2. XRD studies

The most common technique used to identify the corrosion products in the petroleum industry is the X-ray diffraction (XRD) [33]. In order to have basic information of phases present in the corrosion products, XRD patterns were recorded. After being immersed for 30 days in the LAO test solution at 270 ^{o}C and 29 bar, corrosion products of sample CSA516 and the corroded surfaces of SS410 and SS304L were analyzed by XRD. The obtained patterns are depicted in Figs. 8a-8c, respectively.

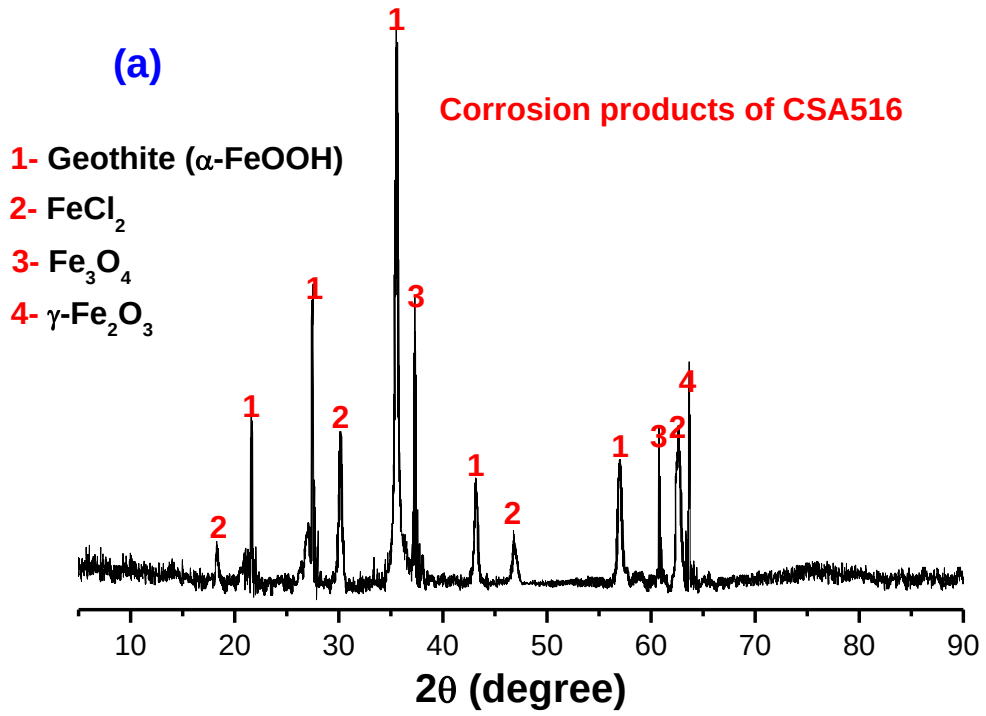
(a)
Corrosion products of CSA516
1- Geothite (α-FeOOH)
2- FeCl2
3- Fe3O4
4- γ-Fe2O3
10
20
30
40
50
60
70
80
90
2θ (degree)

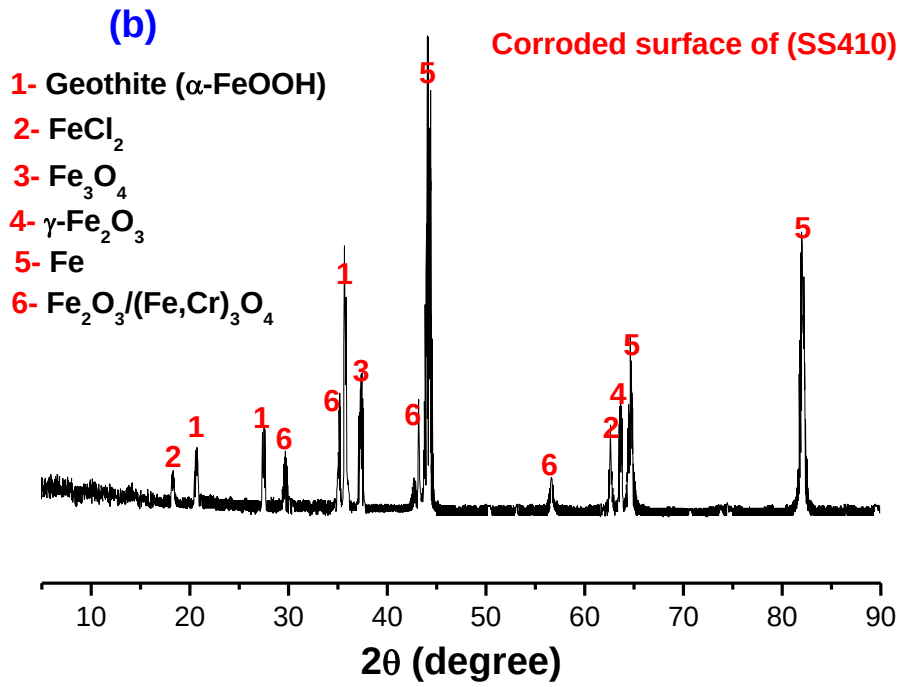
(b)
Corroded surface of (SS410)
1- Geothite (α-FeOOH)
2- FeCl2
3- Fe3O4
4- γ-Fe2O3
5- Fe
6- Fe2O3/(Fe,Cr)3O4
10
20
30
40
50
60
70
80
90
2θ (degree)

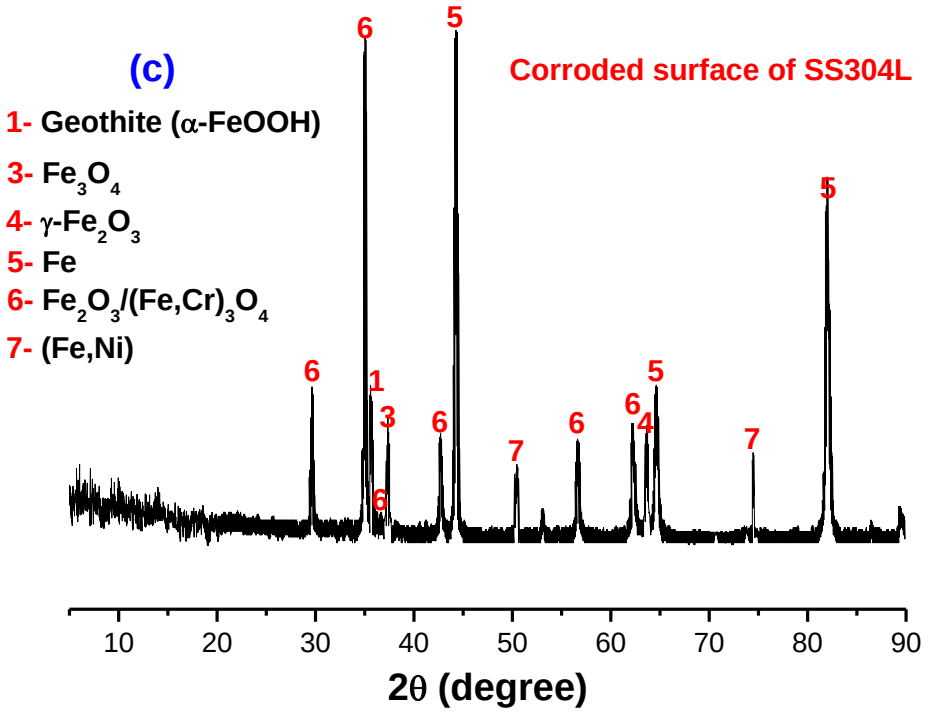

Figure 8. XRD patterns recorded for **(a)** corrosion products of CSA516, **(b)** corroded surface of SS410, and **(c)** corroded surface of SS304L, after 30 days of immersion in the LAO's commercial plant test solution at 270 ^{o}C and 29 bar.

The XRD pattern of the corrosion products of alloy CSA516 (Fig. 8a) displays the presence of a large proportion of geothite (α-FeOOH), as the main phase, which is the expected phase in the case of carbon steel corrosion in chloride environments [33,34], and small amounts of Fe_3O_4, γ-Fe_2O_3, and $FeCl_2$.

On the other hand, the XRD patterns of the corroded surfaces of alloys SS410 (Fig. 8b) and SS304L (Fig. 8c) show the same phases observed previously, but the intensity of the peaks becomes extremely weak compared to those detected in the case of CSA516 (Fig 8a). It is noted that the phase $FeCl_2$ is not detected by the XRD of SS304L, meaning that the corroded surface of SS304L is almost free from such corrosion product, reflecting its higher corrosion resistance as compared to CSA516 and SS410 (see more details in section 4.3). The XRD of SS410 and SS304L also measured, as expected from their Cr contents {(SS410: 12.59% Cr) and (SS304L: 18.43% Cr)}, Table 1, the $(Fe,Cr)_3O_4$ phase. This phase is most likely results from the reaction between the Fe_3O_4 and Cr [35].

The Ni content (7.91%) in 304L is also expected to form Ni oxide films during the corrosion process. However, the Ni oxide structure of this sample is not measured by XRD. It is most likely that Ni oxide films are too thin to be detected by XRD. The Ni is likely to be concentrated at the interface between the oxide and the metal [36].

It can be noted from the comparative patterns shown in Fig. 8a-8c that a significant decrease in the height of the characteristic peaks of geothite, Fe_3O_4, γ-Fe_2O_3, and $FeCl_2$ is observed on going from

CSA516 to SS304L. As the height of the phase peak correlates with its concentration in the sample [37], so the decrease in the height of the corrosion product phases observed in (Figs. 8b and 8c) can be considered as a semi-quantitative indication for the suppression of the corrosion process on the surfaces of SS410 and SS304L as compared with alloy CSA516.

The low corrosion resistance of the carbon steel CSA516 can be further explained based on its microstructure presented in Fig. 9.

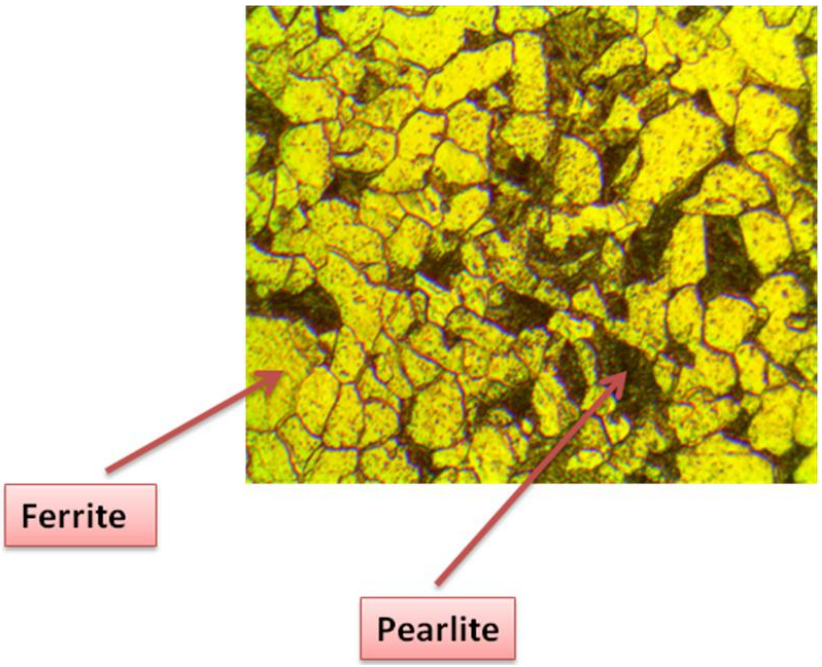

Figure 9. Microstructure of the carbon steel sample CSA516

The optical etched image of sample CSA516 (Fig. 9) shows typical steel microstructure (Ferrite + pearlite). The corrosion resistance of this alloy is very low due to its multiphase structure. The presence of ferrite grains in contact with pearlite ones creates galvanic cells, which in turn enhance the corrosion process. In the same time the pearlite is a mechanical mixture of lamellar ferrite and lamellar iron carbide (cementite). Thus, galvanic cells may also form between the pearlite components, resulting also in accelerated corrosion.

On the other hand, alloys SS410 and SS304L are ferritic and austenitic stainless steels, respectively. The chromium in SS410 (> 12%) and SS304L (> 18%) combines with oxygen in the atmosphere to form a thin, invisible layer of chrome-containing oxide passive film, as confirmed from the formation of $(Fe,Cr)_3O_4$ phase (Figs. 8b and 8c).

The formation and growth of the oxide films on steels can be explained on the basis of the reaction /diffusion controlling mechanism [36]. During the initial stage of the oxidation (corrosion) process, the growth of the oxide film is controlled by the oxidation reaction of metal. This may account for the observed mass loss of these samples (particularly sample CSA516) during the corrosion process. In case of SS410 and SS304L, since Fe and Cr can be oxidized readily by reacting with oxygen to form a barrier layer of Fe and Cr oxides mixed on the sample surface [31], this layer can act

as a barrier against metal and oxygen ion contact. The oxide growth in this stage is governed by the outward diffusion of metal ions and the inward diffusion of oxygen.

The diffusion coefficients of Fe and Cr are much larger than that of oxygen in the barrier layer [36]. Therefore, the growth of the barrier layer is due to the outward diffusion of metal ions. Fe_3O_4 adheres loosely and can leave the substrate easily. However, as a result of the formation of the $(Fe,Cr)_3O_4$, the growth of the oxide layer (i.e., Fe_3O_4) will become compact and protective [36].

In addition, the size of chromium atoms and their oxides are similar, so they pack neatly together on the surface of the metal, forming a stable layer only a few atoms thick [36]. If the metal is cut or scratched and the passive film is disrupted, more oxide will quickly form and recover the exposed surface, protecting it from oxidative corrosion. Iron in alloy CSA516, on the other hand, rusts quickly, as compared with SS410 and SS304L stainless steels, because atomic iron is much smaller than its oxide, so the oxide forms a loose rather than tightly-packed layer and flakes away. These are the reasons why the carbon steel CSA516 recorded the highest corrosion rate, even in presence of the inhibitor, among the tested alloys.

Now we should compare between the corrosion behavior of SS410 and SS304L. The Cr content of SS304L is higher than that of the ferritic stainless steel (SS410). Therefore, the high corrosion resistance of this steel (as confirmed from our chemical tests, inspect figures 6 and 7) may be due to the higher content of $(Fe,Cr)_3O_4$ in the oxide layer, which can decrease the outward diffusion rate of the metal ions. However, the lower Cr content of SS410 as compared with SS304L is insufficient to form the required protective layer. This may be the key reason for the low corrosion resistance of the SS410 steel as compared with SS304L.

In addition, from the microstructure point of view, the high carbon content of alloy SS410 (C: 0.15%), as compared with that of SS304L (C: 0.03%), may be another important factor for the low corrosion resistance of the former. The high carbon content of alloy SS410 gives a real chance for this alloy to form (Fe and Cr carbides) in its microstructure. These carbides also decrease the corrosion resistance of alloy SS410 as compared to SS304L.

The presence of Ni (~8.0%) in SS304L stabilizes the austenite phase, and the structure becomes nearly single phase, and consequently the corrosion resistance increases (no galvanic cells are expected to form) [38]. This behavior is expected to be almost absent in case of our tested ferritic stainless steel (alloy SS410), as its Ni content is less than 1.0%. The low Cr and Ni contents of alloy SS410, in addition to its high carbon content, as compared with SS304L are most likely the reasons why SS410 recorded corrosion rates higher than those of SS304L. Consequently (based on XRD studies, chemical composition and microstructure points of view) the corrosion resistance of the three tested samples enhances in the order: CSA516 < SS410 < SS304L.

4.3. Morphology of the corroded surfaces

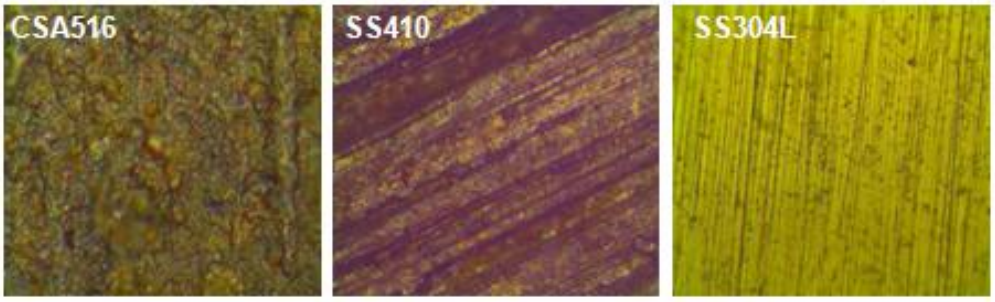

Figure 10. Images of the OM (X200) recorded for the three tested alloys after 30 days of immersion in the LAO test solution at 270 ^{o}C and 29 bar.

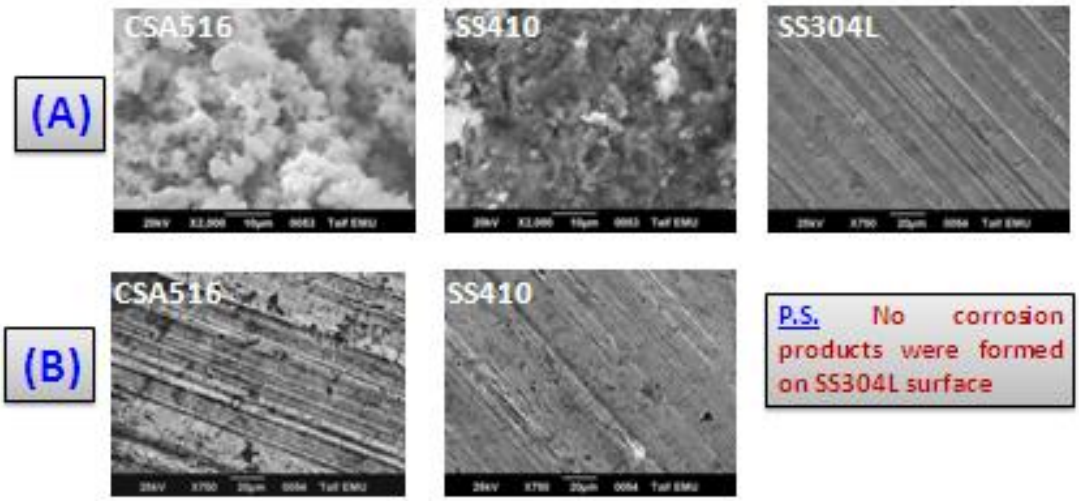

Figure 11. SEM images recorded for the three tested samples after 30 days of immersion in the LAO test solution at 270 ^{o}C and 29 bar. (A): before corrosion products removal (B): After the corrosion products have been removed

The low corrosion resistance of the alloys CSA516 and SS410 is reflected in the large amounts of corrosion products formed on their surfaces. On the other hand, the surface of SS304L is found to be free from such corrosion products; confirming its high corrosion resistance in these solutions. Such morphology data are presented in Figs. 10 and 11.

Optical micrographs (Fig. 10) showed that the surfaces of alloys CSA516 and SS410, after 30 days of immersion in the test solution, were covered with a layer of corrosion product and pitting was not evident. The surface of SS304L is almost free from any corrosion product and pitting attack is not evident too. However, some shallow pits were observed on the surface of SS304L due to the presence of chlorides; the reason why some corrosion rates were recorded for SS304L, as shown in figures 6 and 7.

Based on SEM images (Fig. 11, array A), it can be concluded that, while the corrosion deposits accumulate on the surfaces of the carbon steel sample (CSA516) and the ferritic stainless steel sample (SS410), the surface of the austenitic stainless steels (SS304L) is free from corrosion products.

After the corrosion deposits have been removed (Fig. 11, array B), rough surfaces of CSA516 and SS410 are visualized due to the aggressiveness of the test solution. This surface roughness obviously decreases going from CSA516 to SS304L.

5. CONCLUSION

In view of the above discussion and investigation, the following can be concluded:

(i) The three tested steel samples were found to corrode in the environment of α-Sablin commercial plant based on the inherent properties of the material.

(ii) 304L recorded the highest corrosion resistance among the tested samples, meaning that SS 304L has a relatively high corrosion resistance *vs.* CSA516 and SS410.

(iii) The high Cr and Ni contents of 304L as well as the high stability of the $(Fe,Cr)_3O_4$ mixed oxide phase, as evidenced from XRD, were used to account for its high corrosion resistance, as compared with the other tested alloys.

(iv) The low Cr and Ni contents of alloy 410, in addition to its high carbon content, as compared with 304L are the reasons why 410 recorded corrosion rates higher than those of 304L.

(v) The low corrosion resistance of A516 was explained based on its microstructure. The presence of ferrite grains in contact with pearlite grains in the microstructure of A516 creates galvanic cells. Therefore, accelerated corrosion takes place.

(vi) Surface examination of the corroded surfaces (using OM and SEM) showed that the roughness of the surfaces of the three tested samples decreases following the order: CSA516 < SS410 << SS304L.

References

1. George Lappin, "Alpha Olefins Applications Handbook", CRC Press. ISBN 0-8247-7895-2 (1989).
2. ASTM G1-03 "Standard Practice for Preparing, Cleaning, and Evaluating Corrosion Test" (2011).
3. ANÔNIMO, ASTM G31-72 "Standard Practice for Laboratory Immersion Corrosion Testing of Metals" (1999).
4. M.A. Amin, S.S. Abd El Rehim, M. M. El-Naggar, H.T.M. Abdel-Fatah, *J. Mat. Sci.*, 44 (2009) 6258.
5. H.J. El- Aila, H.M. Tamouse, N.H. Amin, M.A. El- Jboour, *Jordan J. Chem*., 6 (2011) 321.
6. B.A. Salah, M.G. Abd-El-Nasser, A.T. Kandil, *Glob. J. Sci. Front. Res. Chem.*, 12 (2012) 49.
7. A.S Fouda, S. Wanees, A. Modrek, ISRN Metallurgy, Hindawi Publishing Corporation, in press.
8. A.S. Fouda, G.E. Badr, M.N. El-Haddad, *J. Korean Chem. Soc*., 52 (2008) 124.
9. B.A. Lindsley, A.R. Marder, *Wear*, 225–229 (1999) 510.
10. O.K. Abiola, J.O.E. Otaigbe *Corros. Sci*., 51 (2009) 2790.
11. E.M. Sherif, R.M. Erasmus, J.D. Comins, *Corros. Sci*., 50 (2008) 3439.
12. M. Abdallah, M.M. El-Naggar, *Mat. Chem. and Phys*., 71 (2001) 291.
13. M. Abdallah, H.E. Megahed, M. A. Radwan, E. Abdfattah, *J. Am. Sci*., 8 (2012) 49.
14. M. Abdallah, I. Zaafrany, A. Fawzy, M.A. Radwan, E. Abdfattah, J. American Sci., 9, 580-586 (2013).
15. O.A. Hazazi, M. Abdallah, Int. J. Electrochem. Sci., 8, 8138 – 8152 (2013).
16. U. Schulz, M. Peters, Fr.-W Bach, G. Tegeder, Mat. Sci. and Eng. A, 362, 61–80 (2003).
17. N.D. Toniashov, G.P. Chernova, E.N. Ustinski, *Platinum Metals Rev*., 23 (1979) 143.
18. M.A. Amin, *J. Appl. Electrochem*., 36 (2006) 215.
19. M.A. Amin, S.S. Abd El-Rehim, E.E.F. El-Sherbini, R.S. Bayoumi, *Electrochim. Acta* 52 (2007) 3588.
20. M.A. Amin, S.S. Abd EI-Rehim, E.E.F. El-Sherbini, O.A. Hazzazi, M.N. Abbas, *Corros. Sci*., 51 (2009) 658.
21. M.A. Amin, K.F. Khaled, *Corros. Sci*., 52 (2010) 1194.
22. M.A. Amin, K.F. Khaled, S.A. Fadl-Allah, *Corros. Sci*., 52 (2010) 140.
23. M.A. Amin, K.F. Khaled, Q. Mohsen, H.A. Arida, *Corros. Sci*., 52 (2010) 1684.
24. M.A. Amin, O.A. Hazzazi, F. Kandemirli, M. Saracoglu, *Corrosion*, 68 (2012) 688.
25. M.A. Amin, S.S. Abd El Rehim, H.T.M. Abdel-Fatah, *Corros. Sci*., 51 (2009) 882.
26. Song Hong, Wen Chen, Yu Zhang, Hong Qun Luo, Ming Li, Nian Bing Li, *Corrosion Science* 66 (2013) 308–314.
27. N.O. Obi-Egbedi a, I.B. Obot, *Corrosion Science* 53 (2011) 263.
28. M. Behpour, S.M. Ghoreishi, A. Gandomi-Niasar, *J. Mat. Sci.*, 44 (2009) 2444.
29. S. Balaji, A. Upadhyaya, *J. Mat. Sci*., 44 (2009) 2310.
30. G. Sundararajan, P.S. Phani, A. Jyothirmayi, *J. Mat. Sci*., 44 (2009) 2320.
31. V.S. Rao, L.K. Singhal, *J. Mat. Sci*., 44 (2009) 2327.
32. M. Okayasu, K. Sato, K. Okada, *J. Mat. Sci*., 44 (2009) 306.
33. Jenkins R, Snyder RL. Introduction to X-ray Powder Diffractometry, John Willey& Sons Inc., New York, 1996.
34. J. Guo, S. Yang, C. Shang, Y. Wang, X. He, *Corros. Sci*., 51 (2008) 242.
35. N.V. Likhanova, M.A. Dominguez-Aguilar, O. Olivares-Xometl, N. Nava-Entzana, E. Arce, H. Dorantes, *Corros. Sci*. 52 (2010) 2088.
36. X. Gao, X. Wu, Z. Zhang, *J. Supercritical Fluids*, 42 (2007) 157.
37. J. Zhang, N. Li, Y. Chen, *J. Nuclear Materials*, 336 (2005) 1.
38. L. Tan, K. Sridharan, and T. R. Allen, *J. Nuclear Materials*, 348 (2006) 263.